ADVANCED MATERIALS INTERFACES
Open Access
www.advmatinterfaces.de

Combining X-Ray Photoelectron and Absorption Spectroscopies for Determining Surface Chemistry and Composition of $Ti_3C_2T_x$ MXene

Zoé Dessoliers, Arsène Chemin, Geetha Valurouthu, Robert Lord, Thomas Bilyk, Yury Gogotsi, Vincent Mauchamp, and Tristan Petit**

Surface chemistry and core composition of 2D MXenes play a major role in their interfacial properties, but the determination and quantification of their bonding environments remain challenging. X-ray Photoelectron Spectroscopy (XPS) is a method of choice that is broadly utilized but is often hindered by large uncertainties and systematic bias due to adsorbed species such as adventitious carbon or etching residues. In this work, energy-dependent XPS and depth profile modeling of the $Ti_3C_2T_x$ MXene surface are employed to differentiate the contributions from the MXene and the adsorbed species, thereby increasing the accuracy of quantification. In comparison, uncorrected lab-based XPS suffers from a systematic overestimation of Ti vacancies by 7% and an underestimation of terminal atoms, particularly F, by as much as 15%. Interestingly, it is found that a simple inelastic mean free path correction is sufficient to address the issue and reveals extremely low defects in $Ti_3C_2T_x$ MXene synthesized using the HF/HCl etching route. Soft X-ray Absorption Spectroscopy (XAS), supported by Density Functional Theory (DFT) calculations, also demonstrates a high chemical sensitivity of the surface terminations. This work provides novel insights into XPS quantification and the use of XAS for probing the carbide core and surface chemistry of $Ti_3C_2T_x$ MXenes.

1. Introduction

2D transition metal carbides and nitrides, known as MXenes, exhibit a wide spectrum of chemical and physical properties relevant to applications in different fields, such as electrochemical energy storage, electromagnetic interference shielding, catalysis, water purification, and gas separation.[1–9] In all these applications, the surface chemistry of MXenes plays a crucial role by influencing their physicochemical properties. The MXene surface chemistry is mostly determined by the synthesis process, particularly the etching step. Using HF-containing etchants results in MXenes having a mixture of —O, —OH, and —F terminations, while etching with molten chloride salts results in —Cl terminations.[10] Tuning the surface chemistry can significantly modify the electronic and optical properties of MXenes. Indeed, theoretical and experimental studies have demonstrated that for $Ti_3C_2T_x$ (T_x stands for surface terminations) MXene, hydroxyl groups lower the work function[11,12] and increase hydrophilicity,[9] while oxygen terminations play a major role in interband transitions and plasmonic origin,[13] and promote proton transfer.[14] Negatively charged and hydrophilic surfaces of MXenes attract solvated cations (typically, Al remaining from etching and Li from the delamination process) and water molecules. Strongly bonded water between MXene layers can remain within the layers at high vacuum conditions and can only be removed at temperatures well above 200 °C. These intercalated species, along with other atmospheric species that adhere to the surface, make the otherwise reliable characterization of MXene surface chemistry often challenging.

Several techniques are commonly employed to characterize MXene surface chemistry and core composition.[15] Infrared and Raman spectroscopies are sensitive to the bonding of terminal atoms (—O/F/Cl) and the carbide core, but they lack elemental selectivity.[16–19] The elemental selectivity of nuclear magnetic resonance (NMR) is a great asset in providing detailed structural information of MXenes,[20,21] while secondary-ion mass spectrometry (SIMS) offers high atomic sensitivity to study elemental distribution.[22] X-ray Photoelectron Spectroscopy (XPS) is one of the most widely adopted surface-sensitive techniques to

Z. Dessoliers, A. Chemin, T. Petit
Nanoscale Solid-Liquid Interfaces
Helmholtz-Zentrum Berlin für Materialien und Energie GmbH
Albert-Einstein Straße 15, 12489 Berlin, Germany
E-mail: arsene.chemin@univ-lyon1.fr; tristan.petit@helmholtz-berlin.de

A. Chemin
Universite Claude Bernard Lyon 1, CNRS
Institut Lumière Matière, UMR5306
Villeurbanne F-69100, France

G. Valurouthu, R. Lord, Y. Gogotsi
A.J. Drexel Nanomaterials Institute and Department of Materials Science and Engineering
Drexel University
3141 Chestnut St., Philadelphia, PA 19104, USA

T. Bilyk, V. Mauchamp
Université de Poitiers
CNRS, ISAE-ENSMA, PPRIME, Poitiers F-86073, France

The ORCID identification number(s) for the author(s) of this article can be found under https://doi.org/10.1002/admi.202500391

DOI: 10.1002/admi.202500391

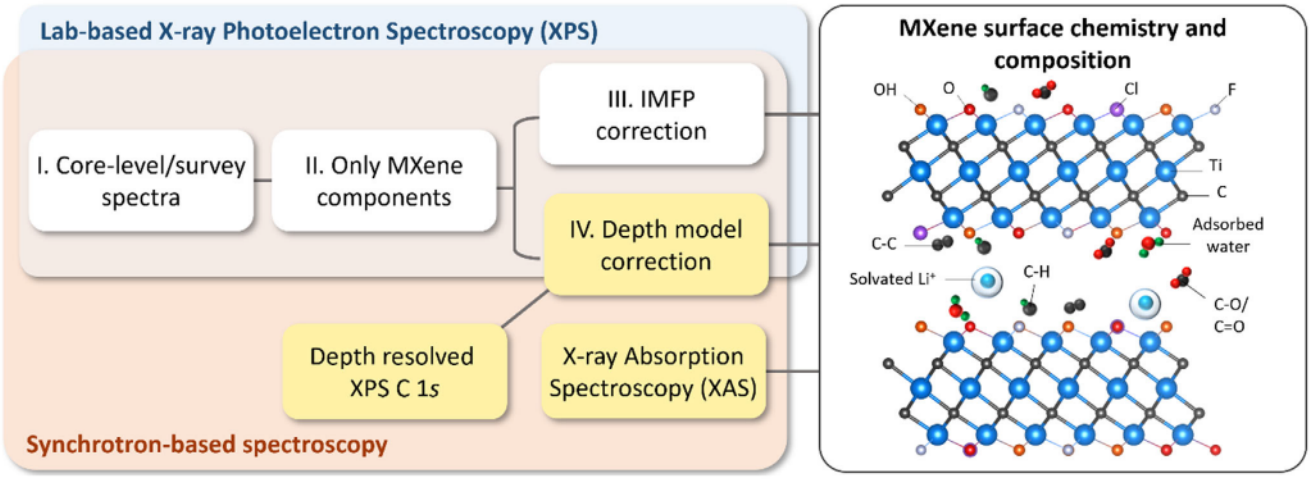

Figure 1. Schematic overview of the step-by-step fitting approach using a combination of X-ray photoemission and absorption spectroscopies. The XPS spectra are fitted to extract the contributions of MXene components onto which the IMFP correction can be applied. Using synchrotron-based XPS, a depth-resolved analysis performed at the C1s core level allows a depth model correction considering surface adsorbates to be compared to the IMFP correction. XAS provides further insights into the bonding environment of the carbide core as well as oxygen and fluorine on the MXene surface.

obtain an element-specific composition and bonding environment of the surface groups. As a result, it has become a go-to technique for MXenes, despite ongoing discussions on spectra interpretation.[21,23–28] One of the main challenges with XPS is that the presence of adventitious carbon (from the atmosphere) on the surface makes the quantification of the carbide and surface terminal groups unreliable. Another challenge is distinguishing the oxygen bonding environments from oxygen on the surface in —O and —OH terminations, strongly adsorbed water, surface contamination, and in the carbon sublattice of non-stoichiometric MXenes.[22] X-ray Absorption Spectroscopy (XAS) is another element-specific technique that probes the unoccupied electronic states of the atoms within the sample, making it highly complementary to XPS. Consequently, XAS with soft X-rays is very sensitive to the oxidation states of transition metals and their chemical environments, as well as light elements such as carbon or nitrogen atoms in the core and oxygen and fluorine in terminal groups on MXenes.[29–33]

In this study, XPS depth profiling–achieved by varying the X-ray excitation energy using a tunable synchrotron light source is introduced to differentiate the contributions from the surface chemistry of $Ti_3C_2T_x$ MXene samples and adsorbed species. By modeling photoemission intensities across different X-ray energies, we accurately determine the type of adsorbed species, as well as the thickness of the adsorbed layer. This approach enables precise quantification of surface terminations, impurities, and the Ti:C ratio in $Ti_3C_2T_x$ MXenes synthesized via mixed-acid (HF/HCl) etching. By employing two etchant compositions with varying HF:HCl ratios, our experimental methodology presented in Figure 1, effectively distinguishes the light elements of the carbide core from surface terminations and contaminants. Additionally, we highlight the high sensitivity of the XAS C K-, O K-, and F K-edges to the MXene surface chemistry, supported by Density Functional Theory (DFT) calculations.

Comparing these results with conventional quantification from laboratory-based XPS using the Al K_α source, we highlight the impact of uncorrected quantification methods. We demonstrate that a straightforward correction based on the inelastic mean free path (IMFP) of electrons, assuming homogeneous samples, effectively mitigates part of the systematic errors. Furthermore, this approach reduces reliance on synchrotron measurements and establishes best practices for laboratory XPS analysis of MXenes.

2. Results and Discussion

2.1. X-ray Photoelectron Spectroscopy (XPS)

2.1.1. Elemental Analysis of the MXene Chemistry by XPS

$Ti_3C_2T_x$ MXenes were synthesized from the high Al-Ti_3AlC_2 MAX phase using the HF/HCl mixed-acid method with different HF concentrations in the etchant, namely 5 and 30 wt.%, and were etched for 24 h (refer to Experimental Section for the detailed synthesis procedure). The corresponding MXenes from the stoichiometric MAX phase are named 5HF- and 30HF-$Ti_3C_2T_x$, respectively. To further support the surface chemistry variations resulting from different etching conditions, MXenes were also synthesized from commercial Ti_3AlC_2 MAX phases following similar etching conditions (5 and 30 wt.% of HF), resulting in a surface chemistry similar to that of stoichiometric $Ti_3C_2T_x$ MXenes, with the relevant data available in the supporting source data file.

XPS survey allows quantification of the atomic ratios of elements present in MXene samples based on the intensity of photoelectrons ejected from their core levels. Figure 2a presents a comparison of XPS survey spectra obtained on the same sample with synchrotron radiation at 750 eV and an Al K_α X-ray source at 1486 eV. The binding energy (BE) of photoelectrons ejected from the core levels of atoms remains fixed in both cases, while the relative intensities and positions of the inelastically scattered and Auger electrons depend on the excitation energy. XPS is highly surface-sensitive and the information depth — defined by the

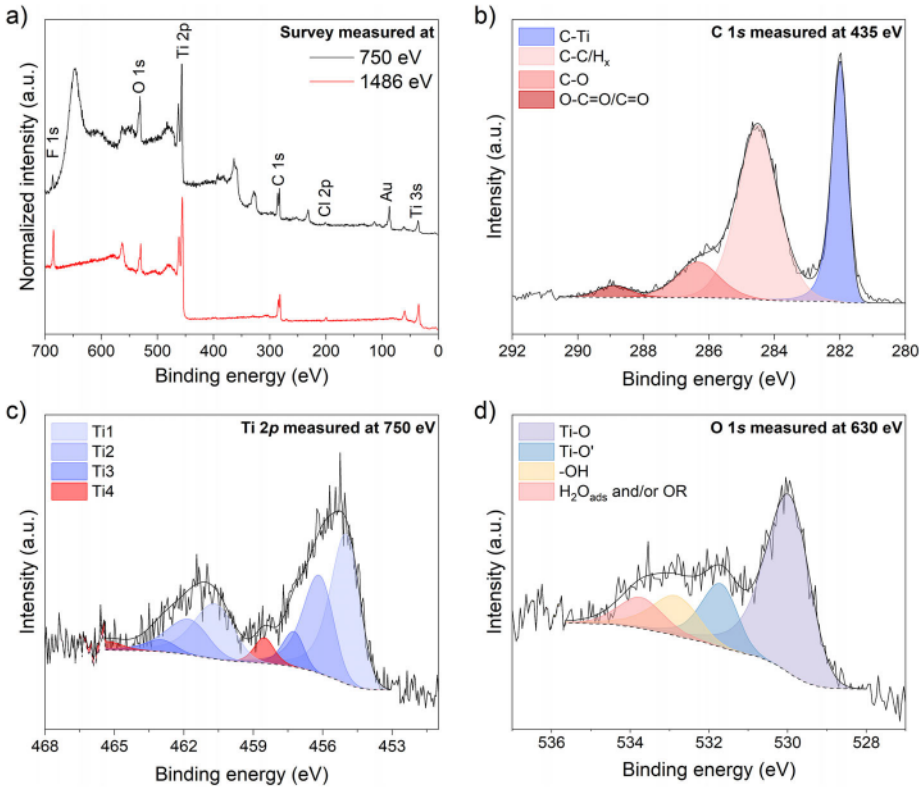

Figure 2. XPS of a) survey spectrum measured with a synchrotron (750 eV, top) and an Al K_α (1486 eV, bottom) source. The spectra are normalized by the Ti 2*p* intensity for easier comparison. b) C 1s, c) Ti 2*p*, d) O 1s spectra measured at 435, 750, and 630 eV, respectively, of 5HF-$Ti_3C_2T_x$ MXene.

IMFP of photoelectrons — is typically only a few nanometers. In particular, the F 1*s* signal appears weaker (2.5 at.%) in the survey obtained at 750 eV compared to the Al K_α source (11.8 at.%), as its kinetic energy ($KE = h\nu - BE$) is smaller (65 eV for 750 eV excitation compared to 801 eV for 1486 eV excitation). As a result, from the universal IMFP approximation in solids,[34] the IMFP of photoelectrons for 750 eV (1486 eV) excitation is ≈0.46 nm (1.52 nm). In the first case, most of the emitted electrons are absorbed by the surface contamination before escaping the sample, especially at the F 1s core level. Therefore, a higher excitation energy is required for a reliable estimation of the fluorine content. Furthermore, for C, O, and Ti core levels, the MXene signature is mixed with signals from adsorbed species, such as adventitious carbon and etching residues. Consequently, identifying and quantifying the surface termination groups as well as obtaining the stoichiometry of the titanium carbide core is affected by sample inhomogeneity, caused mostly by adsorbed species. A simple elemental analysis, performed by correcting the signal intensity of each peak using the relative sensitivity factor (*RSF*) and the transmission (*T*) of the instrument ($I_{corr} = I_{raw}/(RSF \times T)$) yields inconsistent and highly inaccurate atomic concentrations (Table 1). It suggests a non-stoichiometric Ti:C ratio of 0.60 with 750 eV excitation and 0.84 with the Al K_α excitation (Table S5-, Supporting Information) — far lower than the expected ratio of 1.5 — along with an overestimation of carbon and oxygen, which cannot be attributed to MXene core. SIMS measurements were conducted on $Ti_3C_2T_x$ synthesized with 5 wt.% HF and estimated the titanium vacancies (V_{Ti}) concentration to be ≈0.92 ± 0.04 at.%, indicating that V_{Ti} is unlikely to be the cause of the observed non-stoichiometry.[35]

The discrepancy in the stoichiometry of the MXene arises from the presence of adsorbed species on the sample surface and within the interlayer spacing, which may originate from the synthesis process or the storage environment. The layer of adventitious carbon on the surface of the MXene can hardly be avoided during the sample preparation.[36–38] The adsorbed species not only alters the elemental ratios compared to pristine MXene but also affects the signal intensity of each element by absorbing varying amounts of photoelectrons depending on their kinetic energy, as observed for the F 1*s* peak. One typical strategy to reduce surface contamination is to sputter the sample before the XPS measurement, but it induces significant defects in the material and can change the surface composition.[23,28,39] To achieve a more accurate quantification of MXene, the elemental analysis must account for *i)* the signal of MXene components only, and *ii)* IMFP corrections based on the kinetic energy of the electrons or *iii)* the absorption of photoelectrons from the surface contamination (Figure 1). The procedure for these corrections is explained in the next sections and the corrected atomic concentrations and resulting stoichiometries are summarized in Table 1.

2.1.2. XPS Core Level and Survey Fitting

The high-resolution core-level spectra (C 1*s*, Ti 2*p*, and O 1*s*), shown in Figure 2b–d, were recorded using varying excitation

Table 1. Atomic concentrations and stoichiometries obtained from the XPS survey with 750 eV excitation energy and from the XPS core-level spectra with 1486 eV excitation energy. Section (I) integration of full spectral Ti 2*p*, C 1*s*, O 1*s* (that comprises all O species in the sample), F 1*s*, and Cl 2*p* regions without corrections; (II) peak fitting considering solely the MXene components in these spectral regions, with Ti-O and Ti-OH differentiated; (III) application of IMFP corrections assuming a homogeneous sample; and (IV) depth-resolved corrections based on explicit MXene layer thicknesses derived from variable-energy XPS measurements.

	5HF-$Ti_3C_2T_x$								30HF-$Ti_3C_2T_x$							
	Synchrotron XPS [750 eV] at.% from the survey spectrum				Al K_α XPS [1486 eV] at.% from core-level spectra				Synchrotron XPS [750 eV] at.% from the survey spectrum				Al K_α XPS [1486 eV] at.% from core-level spectra			
	I. Full spectral region	II. MXene components	III. IMFP correction	IV. Depth correction	I. Full spectral region	II. MXene components	III. IMFP correction	IV. Depth correction	I. Full spectral region	II. MXene components	III. IMFP correction	IV. Depth correction	I. Full spectral region	II. MXene components	III. IMFP correction	IV. Depth correction
Ti	27.4	34.5	34.7	34.7	31.8	37.7	37.5	37.6	27.8	35.6	36.2	36.3	31.9	37.0	36.8	36.9
C	45.6	30.4	24.3	22.6	37.8	27.1	25.0	24.8	46.1	30.3	24.5	22.8	36.6	26.4	24.3	24.1
O	20.2	24.5	28.2	28.3	17.1	14.6	15.1	15.0	18.8	20.4	23.8	24.0	16.5	13.6	14.0	14.0
OH		1.6	1.8	1.9		4.4	4.5	4.5		3.6	4.2	4.2		4.8	4.9	4.9
F	2.5	3.3	6.7	8.8	11.8	14.4	16.3	16.5	2.1	2.9	6.0	8.0	13.3	16.1	18.1	18.4
Cl	4.3	5.7	4.2	3.7	1.5	1.8	1.6	1.6	5.2	7.1	5.3	4.7	1.7	2.1	1.8	1.8
II. Stoichiometry (MXene components)		$Ti_{2.3}C_2O_{1.6}(OH)_{0.1}F_{0.2}Cl_{0.4}$				$Ti_{2.8}C_2O_{1.1}(OH)_{0.3}F_{1.1}Cl_{0.1}$				$Ti_{2.3}C_2O_{1.3}(OH)_{0.2}F_{0.2}Cl_{0.5}$				$Ti_{2.8}C_2O_1(OH)_{0.4}F_{1.2}Cl_{0.2}$		
III. Stoichiometry (IMFP correction)		$Ti_{2.9}C_2O_{2.3}(OH)_{0.2}F_{0.6}Cl_{0.3}$				$Ti_3C_2O_{1.2}(OH)_{0.4}F_{1.3}Cl_{0.1}$				$Ti_{2.9}C_2O_{1.9}(OH)_{0.3}F_{0.5}Cl_{0.4}$				$Ti_3C_2O_{1.2}(OH)_{0.4}F_{1.5}Cl_{0.2}$		
IV. Stoichiometry (Depth correction)		$Ti_{3.1}C_2O_{2.5}(OH)_{0.2}F_{0.8}Cl_{0.3}$				$Ti_3C_2O_{1.2}(OH)_{0.4}F_{1.3}Cl_{0.1}$				$Ti_{3.2}C_2O_{2.1}(OH)_{0.4}F_{0.7}Cl_{0.4}$				$Ti_{3.1}C_2O_{1.2}(OH)_{0.4}F_{1.5}Cl_{0.1}$		

energies to probe the same MXene volume using the tunable synchrotron X-ray light source. The survey and core-level spectra (C 1*s* and Ti 2*p*) measured on 30HF-$Ti_3C_2T_x$ are shown in Figure S4. The fitting parameters and quantification from the survey and core-level peak fittings for 5HF- and 30HF-$Ti_3C_2T_x$ are provided in Tables S1–S4 (Supporting Information).

The XPS C 1*s* spectrum (Figure 2b) presents four different bonding environments.[23,24,26,28] Only the low-energy peak at 281.9 eV relates to C—Ti bonds from the MXenes, as carbon atoms in $Ti_3C_2T_x$ are only found in one bonding environment, i.e., the octahedral site (Ti—C—Ti). The three other peaks, attributed to C—C/H_x, C—O, and O—C=O/C=O at 284.5, 286.3, and 288.9 eV, respectively, correspond to carbon-containing adsorbed species that are discussed later, and should not be considered in the elemental analysis of the MXenes.

The XPS Ti 2*p* spectrum (Figure 2c) shows the splitting of the 2*p* electronic levels into $2p_{3/2}$ and $2p_{1/2}$. The intensity ratio for the peak fitting is constrained to 2:1. Each set of peaks is composed of three contributions from different bonding environments of the titanium atoms in the MXenes, as recently discussed by Brette et al., based on DFT simulations,[28] and one additional peak at higher binding energy related to oxides. The Ti1 contribution at 454.8 (460.5) eV is attributed to titanium atoms bonded to carbon atoms in the MXene core as well as to $Ti_{surface}$ of unfunctionalized Ti_3C_2. The Ti2 and Ti3 peaks at higher energies, 456.0 (461.6) eV and 457.1 (462.8) eV, respectively, are related to $Ti_{surface}$ bonded to O/F/Cl terminal groups. The Ti2 peak also originates from ejected photoelectrons from Ti_{volume} in $Ti_3C_2O_2$.[28] Finally, the Ti4 bonding environment of titanium atoms at 458.5 (465.3) eV is related to Ti^{4+} chemical state in titanium oxides$_2$)/oxyfluorides ($TiO_{2-x}F_x$),[23,24,26,28] mainly formed at the edges of MXene flakes due to the synthesis conditions and exposure to air, and should not be included in the elemental analysis of MXene. For 5HF-$Ti_3C_2T_x$, this component accounts for only 5.6% of the Ti 2*p* signal, which translates to 1.6 at.% overall, after IMFP correction (Table S1, Supporting Information). Note that this estimation drops down to 3.1% and 1.1 at.% with the Al K_α source, respectively (Table S2, Supporting Information) and no oxide was detected by XRD (Figure S1, Supporting Information), showing that the oxidation is mostly limited to the top MXene surface exposed to air.

The XPS O 1*s* spectrum consists of four peaks (Figure 2d).[23,24,26,28] The most intense peak at 529.8 eV is related to oxygen atoms bonded to surface titanium atoms. Since the Ti 2*p* spectrum reveals the presence of titanium oxide such as TiO_2, titanium oxide also accounts for this peak. The peak at 531.6 eV is ascribed to a Ti—O bond with a disordered surface around the terminating oxygen (noted Ti—O').[28] The peak at 532.7 eV corresponds to -OH terminating groups from the MXene surface or adsorbed on TiO_2 impurities.[24,37,38,40,41] The broad peak at higher energy (533.7 eV) corresponds to adsorbed water and oxygenated carbon contamination (-OR groups). Indeed, from the XRD patterns (Figure S1, Supporting Information), the interlayer space suggests the presence of intercalated water in the MXenes film[15,42] and the XPS C 1*s* spectrum shows a significant amount of carbon-based adsorbed species that contain various bonding environments such as C—O, C=O, and O—C=O. Since the binding energies of the interstitial water, the carbonaceous species, and the titanium oxide are overlapping with peak assigned to MXenes in the O 1*s* spectrum, the quantification of the different oxygen bonding environments remains challenging. We chose to consider the peak related to Ti-O, Ti-O', and —OH in the elemental analysis of MXenes. This assumption is later discussed in the context of the overall corrected quantifications.

In addition, Cl 2*p* and F 1*s* are also detected (Table 1). In the survey, single peaks are observed and are considered to correspond solely to terminal atoms on the MXene, as the samples were thoroughly washed. In particular, the absence of an aluminum signal proves that all the Al from the MAX phase has been removed and that no AlF_3 particles are left from the etching.

The elemental compositions calculated only considering the MXene components from both synchrotron and lab-based XPS measurements are compared in section II of Table 1. The resulting Ti:X ratios with X = C, O, F, OH, Cl are summarized in Table S5 (Supporting Information). This quantification of the MXene components yields a Ti:C ratio of 1.13 for XPS measurements at 750 eV and 1.39 for XPS measured with the Al K_α source, showing a systematic overestimation of the Ti vacancies of 25% and 7% respectively. Although these ratios are much closer to the ideal stoichiometry of MXene after accounting for surface contamination, they still remain inconsistent with other quantitative characterization techniques such as SIMS, which report a vacancy concentration of less than 1 at.% under similar etching conditions.[35] This inaccuracy arises from the absorption of photoelectrons emitted from different depths, which varies with their KE and depends on the element. The phenomenon is emphasized for the synchrotron measurement because the X-ray excitation energy is closer to the BE of the probed elements. As a result, the relative variation of the KE between the elements is larger compared to lab-based XPS, leading to increased errors. Therefore, correction of the electron IMFP should also be applied.

2.1.3. IMFP Correction

The number of photoelectrons detected for a given element *i* corresponds to the electrons escaping the sample surface and can be calculated using the Beer-Lambert law integrated over the sample thickness:

$$N_i = A_i \int \rho_i(z)\, e^{-\frac{z}{\lambda_i(KE)\cos(\alpha)}}\, dz \quad (1)$$

where ρ_i is the atomic density of element *i*, $\lambda_i(KE)$ is the IMFP dependent on the KE, α is the angle between the sample surface normal and the electron analyzer (90° in our case, normal mode emission), and A_i is a proportionality factor that depends on the X-ray photon flux, the RSF, and the analyzer transmission. Since the penetration depth of X-rays is much greater than the IMFP of emitted electrons, the photon flux can be considered constant over the integration.[43] However, the number of detected electrons decreases exponentially with depth *z*, as more photoelectrons are inelastically scattered within the sample.

For a homogeneous sample, where ρ_i does not depend on *z*, Equation (1) can be integrated and $N_i = A_i\, \rho_i \lambda_i(KE)cos(\alpha)$ which explicitly depends on the IMFP of the observed element and the angle between the sample and the electron analyzer. This correction can be directly applied in CasaXPS if the energy correction

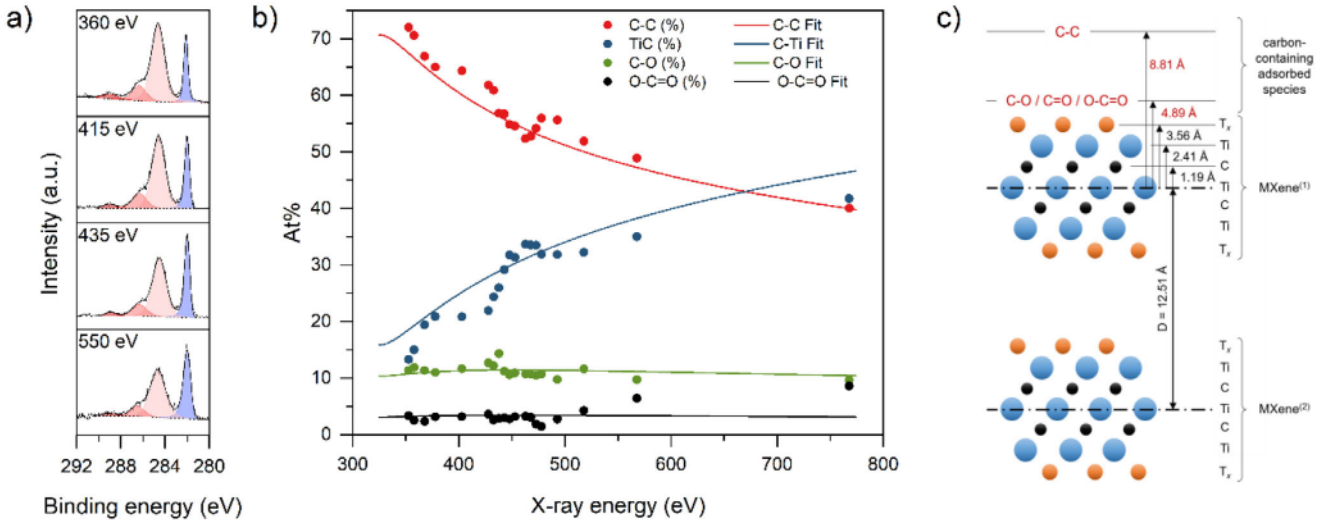

Figure 3. a) XPS core-level C 1s spectra of the 5HF-$Ti_3C_2T_x$ MXene at different X-ray excitation energies, highlighting the change in C-C/C-Ti peak intensity ratios, b) Calculated relative peak fit ratio (%) of the XPS core-level C 1s spectral components measured as a function of incident photon energy and modeled signal (line) and c) Depth model of the MXene and surface contamination with the fit parameters in red.

factor is properly set, or it can be applied a posteriori using, for instance, the universal IMFP approximation in solids.[34] The calculated IMFP values used for MXene in this work are provided in Table S6 (Supporting Information). The elemental analysis from the survey can be corrected using $I_{corr} = I_{raw}/(RSF \times T \times IMFP)$ as shown in Table 1. After correction, the Ti:C ratio is 1.43 at 750 eV and 1.50 at 1486 eV, significantly closer to the expected stoichiometry (Table S5, Supporting Information).

The IMFP correction better corrects the Ti:C stoichiometry for the lab-based XPS. With an excitation energy almost twice as high as the synchrotron source, the volume probed is significantly deeper, i.e., 5–10 nm at 1486 eV, compared to 3–5 nm for an X-ray excitation energy of 750 eV.[44] By probing a deeper volume, the contribution of the adsorbed species is reduced, and the assumption of a homogeneous sample is valid. At the synchrotron, the X-ray excitation energy is lower, increasing surface sensitivity and standard IMFP correction is not sufficient as the MXene inhomogeneity must be considered.

The dependence of probing depth on the KE of the emitted electrons can be mitigated by maintaining a constant KE, which is possible by tuning the X-ray excitation energy from the synchrotron source. This ensures that the probing depth for each element remains similar. However, this approach requires precise calibration of the photon flux and the RSF to achieve accurate elemental quantification. Another way to investigate and correct sample inhomogeneity is to use energy-dependent XPS to achieve depth profiling.

2.1.4. Depth-Resolved Correction

Depth profiling is performed by tuning the X-ray excitation energy from a synchrotron light source. When combined with an analytical model describing the surface chemistry of MXene and the presence of adsorbed species, this approach enables a more precise characterization of bonding environments within the layered structure. To achieve this, we focus exclusively on the C 1*s* signal, as carbon is present in both the MXene and the adsorbed species. A model for a similar XPS depth profiling developed for diamond surfaces was previously reported.[45]

Figure 3a presents the XPS C 1*s* spectra of 5HF-$Ti_3C_2T_x$ MXene at different photon energies. Qualitatively, the contribution from adsorbed species appears more pronounced at lower excitation energies, whereas at higher energies, contributions from atoms located deeper within the material become more prominent (Figure 3b). As the excitation energy increases, the measured concentration of C-Ti rises significantly, while C—O and O—C=O/C=O bonding environments remain relatively constant. Meanwhile, the C—C contribution decreases, indicating that C—C is primarily located at the very surface, followed by C—O and O—C=O/C=O groups beneath it. A model of the depth profile is introduced, consisting of 10 MXene layers (only two are represented in Figure 3c) with a *d*-spacing of 12.5 Å, as determined by XRD (Figure S1a, Supporting Information). In practice, the contribution from C atoms deeper than 5 MXene layers is negligible for the excitation energies used here (IMFP < 15 Å, information depth < 45 Å) as shown in Figure S2 (Supporting Information). The position of the C atoms bonded to Ti within the MXene is set at 1.2 Å from the center of the MXene layer.[46]

The model accounts for contamination that contains two types of carbon from adsorbed species on the sample's surface: i) carbon in the C—C bonding environment and ii) oxygen-containing carbon species, predominantly represented by the C—O and O—C=O/C=O peaks in the C 1*s* spectra.[37,38,47] Some oxygen-containing adsorbed species from the etching and delamination process could also be found in the interlayer spacing, leading to similar results (Figure S3, Supporting Information). Although contamination from sources other than C, such as water and ions, is not explicitly considered, their presence does affect interlayer spacing. For each excitation energy, we quantified the contribution of carbon based on their bonding environment (relative to overall carbon content), which also gives information on

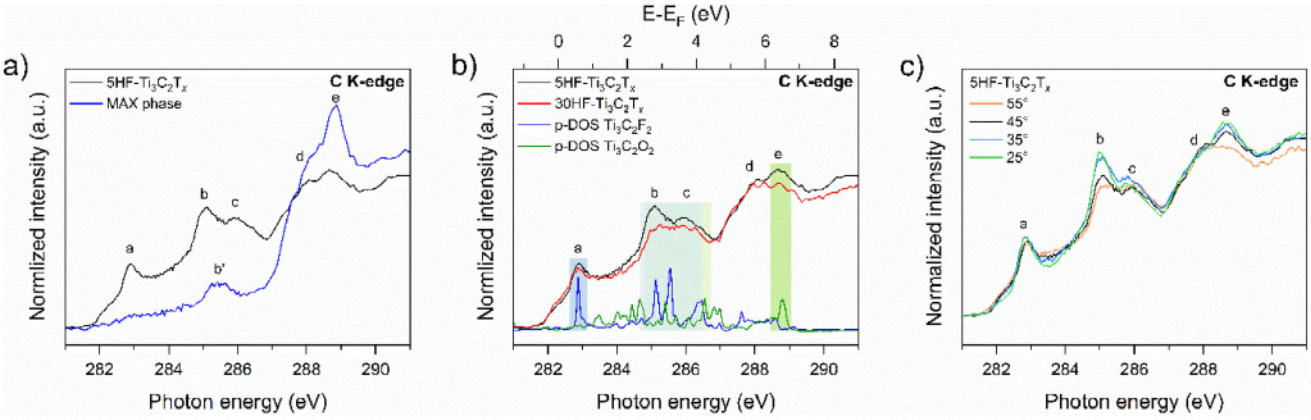

Figure 4. XAS spectra at the C K-edge of a) 5HF-$Ti_3C_2T_x$ MXene (black) and its precursor High-Al Ti_3AlC_2 MAX phase (blue), b) 5HF- (black) and 30HF-$Ti_3C_2T_x$ (red) MXenes compared with the DFT calculated site-projected unoccupied densities of states of p symmetry (p-DOS) for $Ti_3C_2F_2$ (blue) and $Ti_3C_2O_2$ (green), c) angular dependence of the XAS at the C K-edge measured on 5HF-$Ti_3C_2T_x$. The angle corresponds to the angle between the incident X-ray beam and the sample surface.

their relative position to the surface. This was further computed and adjusted with experimental data in Figure 3b. The distance of the oxygen-containing carbon species from the center of the MXene is considered identical for both bounding environments and converges to 4.9 Å while the distance of the C—C species from the center of the MXene converges to 8.8 Å as shown in Figure 3c. This confirms the qualitative analysis presented earlier, with C—C carbon located at the top of the sample. Additionally, this result suggests that polar molecules containing both C—O and O—C═O/C═O groups, along with a C—C carbon segment, may adopt a preferential orientation with the oxygenated species toward the MXene surface. This arrangement could be driven by hydrogen bonding interactions with the MXene oxygen termination groups. The model also determines the ratio of each bonding environment, considering the atomic population of the first MXene and the contamination layer, independent of depth effects. In the first layer, 34.9% of the C 1*s* signal corresponds to carbon atoms from the MXene, 44.2% to C—C carbon, 16.1% to C—O, and 4.8% to O—C═O/C═O groups. In the topmost layer, less than half of the carbon originates from the MXene, confirming that the overestimation of carbon in the uncorrected survey is due to surface contamination.

This model can be used to refine the stoichiometry of the MXene by calculating the signal ratios based on their distance from the surface as reported in section IV of Table 1. The Ti:C ratio corrected this way is 1.53 for the synchrotron measurement and 1.52 for the Al K_α measurement (Table S5, Supporting Information). A slight decrease in the carbon content is observed, which remains within the XPS quantification uncertainties. The overall stoichiometries determined after the depth-resolved corrections are $Ti_{3.1}C_2O_{2.5}OH_{0.2}F_{0.8}Cl_{0.3}$ with the synchrotron source and $Ti_3C_2O_{1.2}OH_{0.4}F_{1.3}Cl_{0.1}$ with the Al K_α source. A similar analysis was performed for 30HF-$Ti_3C_2T_x$, resulting in the stoichiometry of $Ti_{3.2}C_2O_{2.1}OH_{0.4}F_{0.7}Cl_{0.4}$ and $Ti_{3.1}C_2O_{1.2}OH_{0.4}F_{1.5}Cl_{0.1}$ estimated from the synchrotron source and the Al K_α source, respectively (Table 1). This is consistent with the stoichiometries obtained from the IMFP correction (section III of Table 1). Additionally, 30HF-$Ti_3C_2T_x$ has a surface chemistry richer in -F terminations. While the Ti:C ratio remains consistent across both measurements, the surface chemistry composition exhibits variability. The expected stoichiometry of all terminal atoms combined should be 2. However, for 5HF-$Ti_3C_2T_x$, the measured stoichiometries are 3.4 and 3, from the synchrotron and the lab-based XPS measurements after IMFP correction, respectively. Similarly, the stoichiometry of terminal atoms for 30HF-$Ti_3C_2T_x$ also exceeds 2. This variability can arise from uncertainties in the peak assignment or the sample variability, which are discussed in more detail in the Supporting Information. Investigating the bonding environment of the surface states in MXenes is particularly challenging using XPS alone. Therefore, we combine XAS, which is more sensitive to the local atomic environment, with DFT calculations to gain deeper insights.

2.2. X-Ray Absorption Spectroscopy (XAS)

XAS was performed at the C K- (Figure 4), O K-, and F K-edges (Figure 5) to monitor the surface chemistry of 5HF-$Ti_3C_2T_x$ and 30HF-$Ti_3C_2T_x$. The total electron yield (TEY) detection has an information depth of ≈2–4 nm, corresponding to the first 1–3 MXene layers if one accounts for the interlayer spacing.[30] Experimental XAS are compared with DFT calculations for surface chemistry interpretation. The Ti $L_{2,3}$-edge of 5HF-$Ti_3C_2T_x$ and 30HF-$Ti_3C_2T_x$ MXenes (Figure S5, Supporting Information) show a similar signature as previously reported for pristine $Ti_3C_2T_x$.[29,30,48]

The XAS C K-edge spectra (Figure 4a) exhibit five main peaks labeled *a*, *b*, *c*, *d*, and *e* (see full range XAS in Figure S5, Supporting Information) associated with different local environments around the C atoms (i.e., Ti octahedral site). The XAS at the C K-edge corresponds to previously reported C K-edge spectra of $Ti_3C_2T_x$ MXenes.[49,50] The XPS analysis revealed the presence of (oxygenated) carbon-containing adsorbed species. Such species must contribute to the overall C K-edge spectrum of the sample. Indeed, the energy positions of peaks *b*, *d*, and *e* also overlap with typical carbon bonding environments, such as C═C at ≈285.5 eV, O—C═O/C═O at ≈288.7 eV, and O—H/C═O at ≈288.9 eV.[51–53]

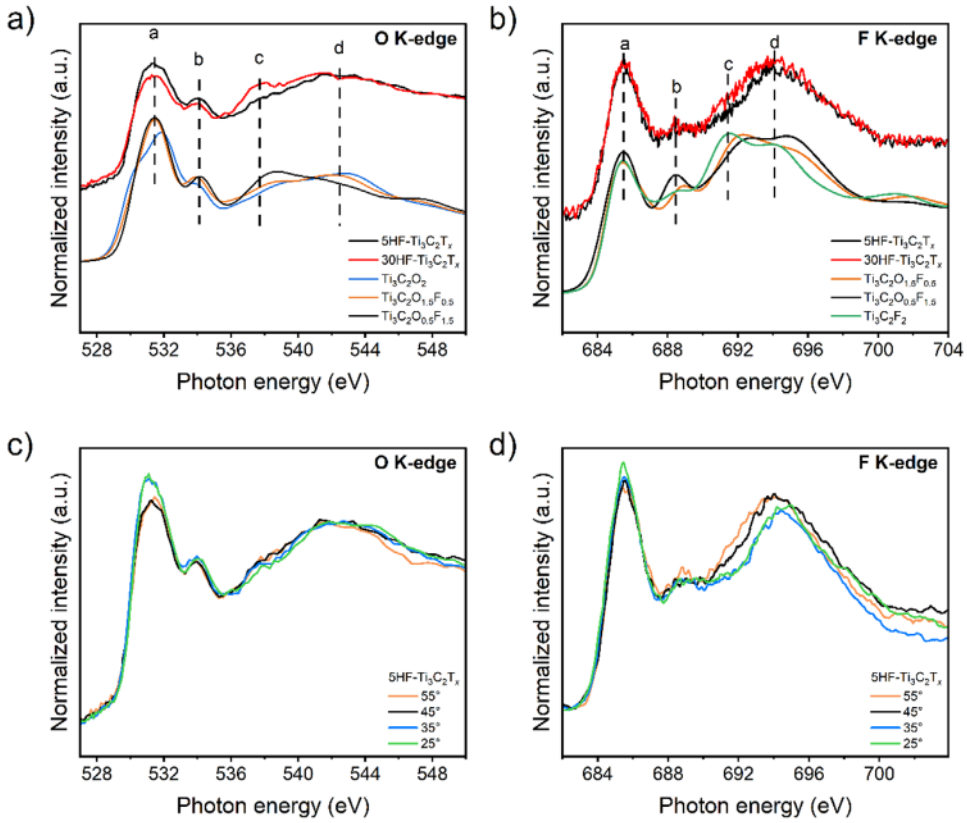

Figure 5. XAS spectra at the a) O K-edge and b) F K-edge of 5HF- and 30HF-$Ti_3C_2T_x$ MXenes. The colored lines at the bottom correspond to DFT calculated EELS spectra from[55] at the a) O K-edge and b) F K-edge of $Ti_3C_2(O_x,F_y)_2$ with different [O]/[F] ratios, c) and d) angular dependence of the O K- and F K-edge measured on 5HF-$Ti_3C_2T_x$, respectively. The angle corresponds to the angle between the incident X-ray beam and the sample surface.

As a result, it is important to analyze the features observed in the XAS C K-edge of MXene with caution.

When comparing the XAS C K-edge spectra of the Ti_3AlC_2 MAX phase and the resulting $Ti_3C_2T_x$ MXene (Figure 4a), clear differences appear that reflect the structural and composition changes after obtaining delaminated MXene. At higher energies, the MAX phase exhibits a relatively sharp and intense peak *e* (288.85 eV), accompanied by a shoulder *d* (287.9 eV). The presence of a common feature in both the MAX and MXene spectra suggests that it originates from structural environments preserved during etching, such as Ti—C—Ti, though its exact spectral features may vary due to changes in the coordination shell of carbon atoms (e.g., Ti—C—Ti—Al vs Ti—C—Ti—O).[54] However, after etching and delamination, the structural environment around carbon becomes more disordered due to the removal of Al layers and the introduction of surface terminations. This increased disorder explains why peaks *d* and *e* appear broader and less intense in the MXene spectrum. In particular, peak *e* shifts slightly to (288.64) eV and loses its sharpness, reflecting changes in the local bonding symmetry and chemical environment of carbon. In the spectrum of the MAX phase, there is also a peak *b'* (285.5 eV), which can also be linked to C—Ti—Al bonding. After etching out the Al and introducing O and F terminations, the MXene spectrum shows two distinct peaks at *b* (285.0 eV) and *c* (286.0 eV). The appearance of *b* and *c* could reflect the influence of surface terminations on the carbon local electronic structure. A new peak also emerges in the MXene at lower energy (282.9 eV, peak *a*), which is not observed in the MAX phase and may be related to surface-related unoccupied electronic states.

The XAS at the C K-edge is compared to the unoccupied DOS calculated by DFT for the two most simple structural models, i.e., $Ti_3C_2O_2$ and $Ti_3C_2F_2$ (Figure 4b) to better understand the influence of the surface chemistry on the C K-edge of MXenes. Despite carbon atoms not being directly bonded to the T_x-groups, the C K-edge shows a high chemical sensitivity to the surface chemistry with clearly distinct contributions coming from —F or —O terminations. Indeed, according to the calculated DOS, peak *a* is solely influenced by the -F terminations, the peaks *b*, *c*, and *d* result from a mixture of —F and —O, and finally the peak *e* is solely related to —O terminations. The measured spectra show that the peaks *a* and *d* seem to be less influenced by a higher number of —F terminations when compared to the other peaks, as the peaks *b*, c, and *e* show significantly reduced contributions for 30HF-$Ti_3C_2T_x$. Considering that peaks *b*, *c*, *d*, and *e* are partially or fully reproduced in the simulated DOS of $Ti_3C_2O_2$, the C K-edge seems to be particularly sensitive to changes in the local environment associated with oxygen terminations, but one should keep in mind the contribution of the adsorbed species in this range of energy.

The angular dependence of the XAS C K-edge of 5HF-$Ti_3C_2T_x$ presented in Figure 4c shows its high sensitivity to the MX-

ene structure. Peaks *a* and *d* exhibit little variation when tilting the beam, while peaks *b*, *c*, and *e* show pronounced intensity variations consistent with differences between 5HF- and 30HF-$Ti_3C_2T_x$. These peaks originate from F-terminations (*a*), a mixture of F and O terminations (*b*, *c*, *d*), and O-terminations (*e*) as discussed above. Different angular dependencies observed for the different terminations may result from changes in the local symmetries, consistent with the fact the Ti—T_x bond lengths are shorter for Ti_s—O (≈1.98 Å) compared to Ti_s—F (≈2.18 Å) according to DFT simulations.[55] Since the C-p states are mixed with the Ti-d states, they reflect such local structural change. The angular dependence of peaks *b*, *c*, and *e* may also be influenced by the contribution of adsorbed species, which have a preferential orientation on the MXene surface as shown by the XPS analysis.

The XAS spectra at the O K- and F K-edges are presented in Figure 5a,b. The XAS spectra lead to generally broader peaks compared to the C K-edge because surface groups are in an intrinsically more disordered environment than the carbide core. Given the very high similarity between the fine structures obtained in XAS and those in EELS, these experiments are compared to the EELS spectra obtained from DFT simulations for different compositions: $Ti_3C_2O_2$, $Ti_3C_2O_{1.5}F_{0.5}$, $Ti_3C_2O_{0.5}F_{1.5}$, and $Ti_3C_2F_2$.[55] Both XAS and EELS indeed probe the site and symmetry projected unoccupied DOS (p-states of the investigated element in the case of a K-edge).

The XAS at the O K-edge (Figure 5a) exhibits four main features labeled *a* (531.4 eV), *b* (534.1 eV), *c* (537.7 eV), and *d* (542.6 eV). This is consistent with previously published EELS data,[55] with an intrinsic higher energy resolution in XAS allowing clear evidence of the peak *b* which is hardly visible in EELS measurements. The peak *a* (531.4 eV) at the O K-edge, assigned to transitions from O 1*s* core levels to O 2*p* levels hybridized with Ti 3*d* states, is less intense for 30HF- than 5HF-$Ti_3C_2T_x$. This reflects a higher oxidation state of the sample in the form of $Ti_3C_2O_2$, as supported by the calculated EELS spectra. DFT simulations are in excellent agreement with the experiments with the four features being well reproduced at similar energies. More careful inspection shows that the best agreement between experiment and theory is obtained for the $Ti_3C_2O_{1.5}F_{0.5}$ composition related to 5HF-$Ti_3C_2T_x$. For 30HF-$Ti_3C_2T_x$, the higher *c* bands agree with a higher F content, as this feature is enhanced for the $Ti_3C_2O_{0.5}F_{1.5}$ theoretical model. The surface chemistry richer in -F terminations 30HF-$Ti_3C_2T_x$ is supported by the XPS. The angular dependence of the O K-edge (Figure 5c) shows a strong dependence on the main peak at 531.4 eV that increases at a lower angle, which agrees with the evolution of the component associated with O-termination at the C K-edge.

At the F K-edge, three main features are clearly visible, labeled *a* (685.5 eV), *b* (688.5), *c* (537.7 eV), and *d* (694.1 eV) in Figure 5b. This XAS spectrum is again very consistent with EELS data from the literature.[55–57] As for the O K-edge, simulations are in good agreement with experiments, with the three main peaks clearly visible. One can however notice that simulations predict a higher relative intensity of the peak *c* which is not observed experimentally. Consistently with the previous analysis at the O K-edge, the best agreement for 5HF-$Ti_3C_2T_x$ is obtained for the $Ti_3C_2O_{1.5}F_{0.5}$ composition where the peak *d* is better positioned as compared to the experiment. For 30HF-$Ti_3C_2T_x$ the peak *c* is slightly more intense, supporting the conclusion that the surface chemistry is richer in -F terminations when compared to the simulation. In contrast with the O K-edge, no clear angular dependence of the main peak *a* is observed for the F K-edge (Figure 5d), as for the F-related component at the C K-edge, confirming the attribution of peak *a* at the C K-edge. The component *c*, on the other hand, shows a significant angular dependency.

Overall, the XAS analysis highlights the high sensitivity of the C K-edge to the MXene surface chemistry, which hence has an impact on the electronic structure of the carbide core. The spectral signature of the O and F K-edges agrees well with the surface chemistry obtained by XPS and seems to be less sensitive to adventitious carbon contamination. The fine structure at the O K-edge also shows clear signatures of local F-enrichment on the MXene surface groups. XAS, therefore, complements XPS well as a surface-sensitive and element-specific technique for the fine characterization of MXene surface chemistry.

3. Conclusion

In this work, the surface composition and stoichiometry of $Ti_3C_2T_x$ MXenes synthesized using the mixed-acid methods (HF/HCl) were analyzed using XPS and XAS. A methodological fitting is proposed to achieve more reliable elemental quantification of the titanium carbide core and of the surface groups by considering only the MXene-related component signals, followed by correcting the inelastic mean free path of electrons and accounting for the surface contamination. Using a synchrotron source, an XPS depth profiling of the MXene film is achieved by tuning the excitation energy. By applying an analytical model to the depth profile, the bonding environments and locations of the carbon-containing adsorbed species, often referred to as adventitious carbon, were identified. The C-C groups are found on the surface, with oxygenated carbons toward the surface of the MXene. These results are compared to lab-based XPS, highlighting the role of the excitation energy on the averaged element quantification of MXenes. XAS is shown to be a highly sensitive tool to probe $Ti_3C_2T_x$ MXene surface chemistry. Through comparison of samples etched in acidic solutions with different HF contents (5HF-$Ti_3C_2T_x$ and 30HF-$Ti_3C_2T_x$), an excellent agreement was observed between XAS and DFT simulations at the C K-, O K- and F K-edges. The general approach presented here for MXenes synthesized by the HF/HCl synthesis route can be further applied to MXenes from different synthesis routes such as etching in LiF/HCl mixtures, molten salt, or electrochemical etching. This work highlights that X-ray spectroscopies are ideally suited to the characterization of MXene chemistry due to their high chemical sensitivity but require additional corrections for the quantitative analysis of the terminal groups and titanium carbide core.

4. Experimental Section

Synthesis: The $Ti_3C_2T_x$ MXenes were obtained from two different Ti_3AlC_2 MAX phases. The results from MXene synthesized from the High-Al Ti_3AlC_2 MAX phase are discussed in the main text. The commercial MAX phase was bought from the company Carbon Ukraine, which produces the MAX phase from a stoichiometric amount of TiC, Al, and Ti powders. This MAX phase and resulting MXenes contain oxygen in the carbon sublattice but have similar surface chemistry. The XPS and XAS results obtained with the commercial MAX phase are available in the

source data file. The "high-Al" stoichiometric Ti_3AlC_2 MAX phase was made from TiC, Al, and Ti powders with an excess of Al and synthesized at Drexel University.[58] It had no traceable oxygen in the carbon sublattice.[22] $Ti_3C_2T_x$ MXene was synthesized and delaminated following the guidelines reported earlier.[59] To etch the MAX phase, the mixed acid etching method was used with 48–51% HF solution in water (Arcos Organics), 9 M HCl (Fisher Chemical), and deionized water in a total volume of 20 mL. The HF:HCl:H_2O volume ratios were 2:8:10 and 12:8:0 for 5HF-$Ti_3C_2T_x$ and 30HF-$Ti_3C_2T_x$, respectively. Lithium chloride (LiCl) in deionized water was used to delaminate the multilayered $Ti_3C_2T_x$ MXenes.

Film preparation: Films for XRD and XPS (Al K_α source) were prepared by vacuum-assisted filtration. Freestanding MXene films were obtained from the colloidal suspension of collected delaminated MXenes with single to few-layer flakes by vacuum-assisted filtration through a porous membrane (Celgard 3501, 64 nm pore size, polypropylene). The films were carefully separated from the Celgard and stored in a sterile plastic Petri dish at room temperature.

Films for XAS and XPS analysis in synchrotron were prepared by spray-coating. The MXene films were spray-coated on the gold-coated p-Si substrate to ensure good conductivity and free the measurement from the silicon oxide layer signal. Before spray-coating, the substrates were washed, sonicated, and then dried with N_2 compressed gas and Ar/O_2 plasma treated (Tergeo Plus, Pie Scientific) to make the surface hydrophilic. The pre-treated slides were spray-coated with $Ti_3C_2T_x$ colloidal suspension (≈1 mg.mL^{-1}) with various numbers of deposition and an operating distance of ≈20 cm between the spray nozzle and the substrate, followed by air drying through a hair dryer (1875, Conair). The MXene films (≈20 µm thick) were stored in a glove box filled with Ar.

Characterization Techniques: X-Ray Diffraction (XRD). A Rigaku Miniflex X-ray diffractometer (Rigaku Corporation, JP) was used to perform the XRD analysis on the $Ti_3C_2T_x$ MXene and Ti_3AlC_2 MAX phases samples. A Cu $K_{\alpha 1}$ radiation source (1.5406 Å) was used at 40 kV/15 mA. The scans were recorded from 3° to 60° with a step size of 0.02° and a step duration of 0.4 s.

UV–vis Spectroscopy: The optical properties of the MXenes were investigated with UV–vis–NIR.[60] The UV–vis–NIR spectra were recorded using an Evolution 201 spectrometer (Thermo Scientific) in transmission mode with a 10 mm optical path length quartz cuvette. The absorbance was measured from 200 to 1100 nm on MXene solutions after multiple dilutions, and DI water was used for the blank.

X-Ray Photoelectron Spectroscopy (XPS): XPS spectra were performed at the BESSY II synchrotron facility using the HE-SMG experimental station equipped with aR3000 electron energy analyzer (Scienta).[61] The energy of the probing photons was tuned using a monochromator. The XPS surveys were performed using an incident energy of 750 eV. The energy resolution of the monochromator combined with the hemispherical detection measuring conditions, the photoelectron energy resolution was better than 0.5 eV, which was estimated to be smaller than the natural width of the C 1s core levels, resulting in XP line shapes measurements of high chemical sensitivity. Indeed, great care has been taken during and after the sample preparation to remain in a clean environment and inert gas, except for the loading under vacuum as the sample has been exposed to air for less than a minute.The lab-based XPS data were collected from freestanding films using a PHI VersaProbe 5000 instrument (Physical Electronics, U.S.) with a 200 µm spot size and 50 W monochromatic Al-K_α X-ray source corresponding to 1486 eV photon energy. Pass energy and step size were set at 23.5 and 0.05 eV, respectively. For the C 1s spectra, the C-Ti peak was positioned at 282.0 eV to account for shifts due to the homogeneous charging of the sample. For the peak fitting of the Ti 2*p* spectra, the intensity ratios of the $2p_{3/2}$ and $2p_{1/2}$ components were constrained to be 2:1. Quantification and peak fitting were conducted using CasaXPS V2.3.19 Software. A detailed description of the curve fitting can be found in the Supporting Information.

X-Ray Absorption Spectroscopy (XAS): XAS was performed using the same endstation by sweeping the X-ray wavelengths using the monochromator and measuring the absorption simultaneously using the total electron yield (TEY) mode by recording the emitted electrons from the sample under a 30 V retarding potential. The screening potential selects the electrons with high energy and increases the surface sensitivity of the technique, estimated to a few tens of nanometers. The HE-SMG beamline optical scheme has been optimized to limit carbon contamination on the beamline's optical elements, so no reference background subtraction is required—even at the C K-edge—though a standard linear background correction was still applied. The spectra were normalized by the incident photon flux and between the pre-edge and post-edge regions. The energy resolution of the monochromator in the range of the C 1s (≈285 eV) X-ray absorption edges was ≈100 meV.[62] The XAS at the C K-edge was calibrated against the energy positions of the first narrow peak of the C 1s absorption spectrum of highly ordered pyrolytic graphite (HOPG) (≈285.45 eV). The XAS at the Ti L-edge and O K-edge were calibrated in energy according to the literature.[30,48,63] The XAS spectra at the F K-edge could not be calibrated in energy as no previous report of $Ti_3C_2T_x$ MXene XAS spectrum at the F K-edge was reported in the literature to our knowledge. The onset of the F K-edge was positioned accordingly to simulate and measure EELS spectra at the F K-edge by Bilyk et al., which was consistent with the calibration applied on the O K-edge spectra when compared to EELS spectra.[55]

Density Functional Theory (DFT): DFT simulations were performed as described by Bilyk et al.[55] In brief, the all-electron, full potential augmented-plane-wave (APW) method as implemented in the WIEN2k code was used[64] and calculations were performed in the generalized gradient approximation using the Perdew-Burke-Ernzerhof (GGA-PBE) exchange and correlation functional.[65] All simulation parameters can be found in ref. [55] and EEL spectra were calculated using the TELNES program of WIEN2k.[66] $Ti_3C_2T_2$ structural models (T=O or F or a mixture of those) were considered, with the T_x-groups sitting in the fcc position. In order to account for the excitation process (i.e., the removal of an electron from the 1s orbital in the case of a K-edge), simulations were performed in the final state approximation, i.e., including a core hole on the investigated atom. To avoid the interaction of the core hole with its repeated image due to periodic boundary conditions, 2×2×1 supercells were necessary. For comparison to experiments, the energy positions of the theoretical spectra were adjusted so that the Fermi level, or the edge onset, match the experimental edge onset. A slight rigid shift correction was then applied to refine the positions of the simulated peaks to match the experimental ones. This correction can be understood from the fact that the position of the theoretical Fermi level might not exactly match the experimental one due to, e.g., the difference between the ideal $Ti_3C_2T_2$ systems considered in the calculations and the more complex chemistry of the real samples.

Supporting Information

Supporting Information is available from the Wiley Online Library or from the author.

Acknowledgements

Z.D and A.C. contributed equally to this work. Z.D. and A.C. are first co-authors. This project received funding from the European Research Council (ERC) under the European Union's Horizon 2020 research and innovation program (grant agreement No 947852). The authors thank the Helmholtz-Zentrum Berlin fur Materialien und Energie for the allocation of synchrotron radiation beamtime. The help from Maria Brzhezinskaya at the beamline HE-SGM was greatly appreciated. The authors acknowledge financial support from the "Région Nouvelle Aquitaine" for the Ph.D. thesis of T.B. Computations have been performed on the supercomputer facilities of the "Mésocentre de calcul de Poitou Charentes". This work was supported by the French government program "Investissements d'Avenir" (EUR INTREE: ANR-18-EURE-0010; LABEX INTERACTIFS: ANR-11-LABX-0017-01). MXene development and characterization at Drexel University was supported by the U.S. National Science Foundation under Grant CHE-2318105 (M-STAR CCI).

Conflict of Interest

The authors declare no conflict of interest.

Data Availability Statement

The data that support the findings of this study are openly available in Zenodo at https://doi.org/10.5281/zenodo.15296289, reference number 15296290.

Keywords

density functional theory, MXene, soft X-ray absorption spectroscopy, surface chemistry, X-ray photoelectron spectroscopy

Received: May 2, 2025
Revised: May 28, 2025
Published online: June 16, 2025

[1] M. Naguib, O. Mashtalir, J. Carle, V. Presser, J. Lu, L. Hultman, Y. Gogotsi, M. W. Barsoum, *ACS Nano* **2012**, *6*, 1322.
[2] B. Anasori, Y. Gogotsi, *Graphene 2D Mater* **2023**, *8*, 39.
[3] S. Kajiyama, L. Szabova, K. Sodeyama, H. Iinuma, R. Morita, K. Gotoh, Y. Tateyama, M. Okubo, A. Yamada, *ACS Nano* **2016**, *10*, 3334.
[4] M. Okubo, A. Sugahara, S. Kajiyama, A. Yamada, *Acc. Chem. Res.* **2018**, *51*, 591.
[5] K. Kawai, M. Fujita, R. Iizuka, A. Yamada, M. Okubo, *2D Mater* **2023**, *10*, 014012.
[6] F. Shahzad, M. Alhabeb, C. B. Hatter, B. Anasori, M. Hong, C. M. Koo, Y. Gogotsi, *Science* **2016**, *353*, 1137.
[7] I. Persson, J. Halim, H. Lind, T. W. Hansen, J. B. Wagner, L. Näslund, V. Darakchieva, J. Palisaitis, J. Rosen, P. O. Å. Persson, *Adv. Mater.* **2019**, *31*, 1805472.
[8] J. Lu, I. Persson, H. Lind, J. Palisaitis, M. Li, Y. Li, K. Chen, J. Zhou, S. Du, Z. Chai, Z. Huang, L. Hultman, P. Eklund, J. Rosen, Q. Huang, P. O. Å. Persson, *Nanoscale Adv.* **2019**, *1*, 3680.
[9] J. Hart, K. Hantanasirisakul, A. C. Lang, B. Anasori, D. Pinto, Y. Pivak, J. T. van Omme, S. J. May, Y. Gogotsi, M. L. Taheri, *Nat. Commun.* **2019**, *10*, 522.
[10] Y. Li, H. Shao, Z. Lin, J. Lu, L. Liu, B. Duployer, P. O. Å. Persson, P. Eklund, L. Hultman, M. Li, K. Chen, X. Zha, S. Du, P. Rozier, Z. Chai, E. Raymundo-Piñero, P.-L. Taberna, P. Simon, Q. Huang, *Nat. Mater.* **2020**, *19*, 894.
[11] M. Khazaei, M. Arai, T. Sasaki, A. Ranjbar, Y. Liang, S. Yunoki, *Phys. Rev. B* **2015**, *92*, 075411.
[12] T. Schultz, P. Bärmann, E. Longhi, R. Meena, Y. Geerts, Y. Gogotsi, S. Barlow, S. R. Marder, T. Petit, N. Koch, *Phys. Rev. Mater.* **2023**, *7*, 45002.
[13] A. Furchner, T. Parker, V. Mauchamp, S. Hurand, J. Plaickner, J. Rappich, A. A. Emerenciano, K. Hinrichs, Y. Gogotsi, T. Petit, *J. Phys. Chem. C* **2025**, *129*, 500.
[14] H. Shao, K. Xu, Y.-C. Wu, A. Iadecola, L. Liu, H. Ma, L. Qu, E. Raymundo-Piñero, J. Zhu, Z. Lin, P.-L. Taberna, P. Simon, *ACS Energy Lett.* **2020**, *5*, 2873.
[15] M. Shekhirev, C. E. Shuck, A. Sarycheva, Y. Gogotsi, *Prog. Mater. Sci.* **2021**, *120*, 100757.
[16] A. Sarycheva, Y. Gogotsi, *Chem. Mater.* **2020**, *32*, 3480.
[17] E. Berger, Z. P. Lv, H. P. Komsa, *J. Mater. Chem. C* **2022**, *11*, 1311.
[18] T. Parker, D. Zhang, D. Bugallo, K. Shevchuk, M. Downes, G. Valurouthu, A. Inman, B. Chacon, T. Zhang, C. E. Shuck, Y.-J. Hu, Y. Gogotsi, *Chem. Mater.* **2024**, *36*, 8437.
[19] J. Plaickner, T. Petit, P. Bärmann, T. Schultz, N. Koch, N. Esser, *Phys. Chem. Chem. Phys.* **2024**, *26*, 20883.
[20] M. Anayee, N. Kurra, M. Alhabeb, M. Seredych, M. N. Hedhili, A.-H. Emwas, H. N. Alshareef, B. Anasori, Y. Gogotsi, *Chem. Commun.* **2020**, *56*, 6090.
[21] F. Brette, D. Kourati, M. Paris, L. Loupias, S. Célérier, T. Cabioc'h, M. Deschamps, F. Boucher, V. Mauchamp, *J. Am. Chem. Soc.* **2023**, *145*, 4003.
[22] P. P. Michalowski, M. Anayee, T. S. Mathis, S. Kozdra, A. Wójcik, K. Hantanasirisakul, I. Jozwik, A. Piatkowska, M. Mozdzonek, A. Malinowska, R. Diduszko, E. Wierzbicka, Y. Gogotsi, *Nat. Nanotechnol.* **2022**, *17*, 1192.
[23] J. Halim, K. M. Cook, M. Naguib, P. Eklund, Y. Gogotsi, J. Rosen, M. W. X. Barsoum, *Appl. Surf. Sci.* **2016**, *362*, 406.
[24] L.-Å. Näslund, P. O. Å. Persson, J. Rosen, *J. Phys. Chem. C* **2020**, *124*, 27732.
[25] I. Persson, L.-Å. Näslund, J. Halim, M. W. Barsoum, V. Darakchieva, J. Palisaitis, J. Rosen, P. O. Å. Persson, *2D Mater.* **2017**, *5*, 015002.
[26] L. Loupias, C. Morais, S. Morisset, C. Canaff, Z. Li, F. Brette, P. Chartier, N. Guignard, L. Maziere, V. Mauchamp, T. Cabioc'h, A. Habrioux, S. Célérier, *FlatChem* **2024**, *43*, 100596.
[27] T. Schultz, N. C. Frey, K. Hantanasirisakul, S. Park, S. J. May, V. B. Shenoy, Y. Gogotsi, N. Koch, *Chem. Mater.* **2019**, *31*, 6590.
[28] F. Brette, S. Célérier, C. Canaff, L. Loupias, M. Paris, A. Habrioux, F. Boucher, V. Mauchamp, *Small Methods* **2024**, *9*, 2400848.
[29] A. Al-Temimy, B. Anasori, K. A. Mazzio, F. Kronast, M. Seredych, N. Kurra, M.-A. Mawass, S. Raoux, Y. Gogotsi, T. Petit, *J. Phys. Chem. C* **2020**, *124*, 5079.
[30] F. Amargianou, P. Bärmann, H. Shao, P.-L. Taberna, P. Simon, J. Gonzalez-Julian, M. Weigand, T. Petit, *Small Methods* **2024**, *8*, 2400190.
[31] Y. Xie, M. Naguib, V. N. Mochalin, M. W. Barsoum, Y. Gogotsi, X. Yu, K.-W. Nam, X.-Q. Yang, A. I. Kolesnikov, P. R. C. Kent, *J. Am. Chem. Soc.* **2014**, *136*, 6385.
[32] M. R. Lukatskaya, S. M. Bak, X. Yu, X. Q. Yang, M. W. Barsoum, Y. Gogotsi, *Adv. Energy Mater.* **2015**, *5*, 1500589.
[33] Y. Lu, D. Li, F. Liu, *Materials* **2022**, *15*, 307.
[34] M. P. Seah, W. A. Dench, *Surf. Interface Anal.* **1979**, *1*, 2.
[35] B. C. Wyatt, M. G. Boebinger, Z. D. Hood, S. Adhikari, P. P. Michalowski, S. K. Nemani, M. G. Muraleedharan, A. Bedford, W. J. Highland, P. R. C. Kent, R. R. Unocic, B. Anasori, *Nat. Commun.* **2024**, *15*, 6353.
[36] G. Greczynski, L. Hultman, *ChemPhysChem* **2017**, *18*, 1507.
[37] J. Balajka, M. A. Hines, W. J. I. DeBenedetti, M. Komora, J. Pavelec, M. Schmid, U. Diebold, *Science* **2018**, *361*, 786.
[38] L. H. Grey, H. Y. Nie, M. C. Biesinger, *Appl. Surf. Sci.* **2024**, *653*, 159319.
[39] M. Ghidiu, J. Halim, S. Kota, D. Bish, Y. Gogotsi, M. W. Barsoum, *Chem. Mater.* **2016**, *28*, 3507.
[40] S. Yamamoto, H. Bluhm, K. Andersson, G. Ketteler, H. Ogasawara, M. Salmeron, A. Nilsson, *J. Phys. Condens. Matter* **2008**, *20*, 184025.
[41] M. Schied, H. Pazniak, F. Brette, P. Lacovig, M. Paris, F. Boucher, S. Lizzit, V. Mauchamp, R. Larciprete, *Chem. Mater.* **2024**, *36*, 11905.
[42] Y. Sun, C. Zhan, P. R. C. Kent, M. Naguib, Y. Gogotsi, D. Jiang, *ACS Appl. Mater. Interfaces* **2020**, *12*, 763.
[43] T. Petit, M. Lounasvuori, A. Chemin, P. Bärmann, *ACS Phys. Chem. Au* **2023**, *3*, 263.
[44] M. Gawek, S. Madkour, P. Szymoniak, J. Radnik, A. Schönhals, *Soft Matter* **2021**, *17*, 6985.
[45] A. Chemin, M. K. Kuntumalla, M. Brzhezinskaya, T. Petit, A. Hoffman, *Appl. Surf. Sci.* **2024**, *661*, 160082.
[46] C. Shi, M. Beidaghi, M. Naguib, O. Mashtalir, Y. Gogotsi, S. J. L. Billinge, *Phys. Rev. Lett.* **2013**, *112*, 125501.
[47] G. Greczynski, L. Hultman, *Vacuum* **2022**, *205*, 111463.

[48] Y. Yang, K. Hantanasirisakul, N. C. Frey, B. Anasori, R. J. Green, P. C. Rogge, I. Waluyo, A. Hunt, P. Shafer, E. Arenholz, V. B. Shenoy, Y. Gogotsi, S. J. May, *2D Mater* **2020**, *7*, 025015.
[49] Y. Zhang, H. Jiang, Y. Lin, H. Liu, Q. He, C. Wu, T. Duan, L. Song, *Adv. Mater. Interfaces* **2018**, *5*, 1800392.
[50] X. Cao, Y. Liu, H. Xia, Y. Li, L. Yang, H. Wang, H. Zhang, B. Ye, W. He, T. Wei, Z. Xin, C. Lu, M. Zhou, Z. Sun, *Adv. Mater.* **2024**, *36*, 2408723.
[51] J. Ren, F. Weber, F. Weigert, Y. Wang, S. Choudhury, J. Xiao, I. Lauermann, U. Resch-Genger, A. Bande, T. Petit, *Nanoscale* **2019**, *11*, 2056.
[52] R. P. Gandhiraman, D. Nordlund, C. Javier, J. E. Koehne, B. Chen, M. Meyyappan, *J. Phys. Chem. C* **2014**, *118*, 18706.
[53] C.-H. Chuang, S. C. Ray, D. Mazumder, S. Sharma, A. Ganguly, P. Papakonstantinou, J.-W. Chiou, H.-M. Tsai, H.-W. Shiu, C.-H. Chen, H. Lin, J. Guo, W.-F. Pong, *Sci. Rep.* **2017**, *7*, 42235.
[54] M. Bugnet, V. Mauchamp, P. Eklund, M. Jaouen, T. Cabioc'h, *Acta Mater.* **2013**, *61*, 7348.
[55] T. Bilyk, M. Benchakar, M. Bugnet, L. Loupias, P. Chartier, H. Pazniak, M.-L. David, A. Habrioux, S. Celerier, J. Pacaud, V. Mauchamp, *J. Phys. Chem. C* **2020**, *124*, 27071.
[56] D. Magne, V. Mauchamp, S. Célérier, P. Chartier, T. Cabioc'h, *Phys. Chem. Chem. Phys.* **2016**, *18*, 30946.
[57] J. K. El-Demellawi, S. Lopatin, J. Yin, O. F. Mohammed, H. N. Alshareef, *ACS Nano* **2018**, *12*, 8485.
[58] T. S. Mathis, K. Maleski, A. Goad, A. Sarycheva, M. Anayee, A. C. Foucher, K. Hantanasirisakul, C. E. Shuck, E. A. Stach, Y. Gogotsi, *ACS Nano* **2021**, *15*, 6420.
[59] M. Downes, C. E. Shuck, B. McBride, J. Busa, Y. Gogotsi, *Nat. Protoc.* **2024**, *19*, 1807.
[60] K. Maleski, C. E. Shuck, A. T. Fafarman, Y. Gogotsi, *Adv. Opt. Mater.* **2021**, *9*, 2001563.
[61] A. Nefedov, C. Wöll, in *Surface Science Techniques* (eds: G. Bracco, B. Holst), Springer Series in Surface Sciences, vol. *51*, Springer, Berlin, Germany **2013**, pp. 277–303.
[62] M. Sobaszek, M. Brzhezinskaya, A. Olejnik, V. Mortet, M. Alam, M. Sawczak, M. Ficek, M. Gazda, Z. Weiss, R. Bogdanowicz, *Small* **2023**, *19*, 2208265.
[63] A. Al-Temimy, K. Prenger, R. Golnak, M. Lounasvuori, M. Naguib, T. Petit, *ACS Appl. Mater. Interfaces* **2020**, *12*, 15087.
[64] P. Blaha, K. Schwarz, F. Tran, R. Laskowski, G. K. H. Madsen, L. D. Marks, *J. Chem. Phys.* **2020**, *152*, 074101.
[65] J. P. Perdew, K. Burke, M. Ernzerhof, *Phys. Rev. Lett.* **1996**, *77*, 3865.
[66] C. Hébert, *Micron* **2007**, *38*, 12.